Geochimica et Cosmochimica Acta 382 (2024) 118–127

Contents lists available at ScienceDirect

Geochimica et Cosmochimica Acta

journal homepage: www.elsevier.com/locate/gca

Isotopic evidence for a common parent body of IIG and IIAB iron meteorites

Aryavart Anand [a,b,*], Fridolin Spitzer [a], Timo Hopp [a,c], Richard Windmill [d], Pascal Kruttasch [b], Christoph Burkhardt [a], Nicolas Dauphas [c], Richard Greenwood [d], Beda Hofmann [b,e], Klaus Mezger [b], Thorsten Kleine [a]

[a] Max Planck Institute for Solar System Research, Göttingen 37077, Germany
[b] Institut für Geologie, Universität Bern, Bern 3012, Switzerland
[c] Origins Laboratory, Department of the Geophysical Sciences and Enrico Fermi Institute, The University of Chicago, Chicago, IL 60637, USA
[d] Planetary and Space Sciences, The Open University, Milton Keynes MK7 6AA, UK
[e] Naturhistorisches Museum Bern, Bern 3005, Switzerland

ARTICLE INFO

Associate editor: Audrey Bouvier

Keywords:
Magmatic iron meteorites
Isotopic anomalies
Core formation

ABSTRACT

Magmatic iron meteorites are thought to sample the metallic cores of differentiated planetesimals and are subdivided into several chemical groups, each representing a distinct parent body. The only exceptions are the groups IIAB and IIG, which have been proposed to sample two immiscible melts from the same core. To test this model, we report the first Fe, Ni, O, and Cr isotope data for IIG iron meteorites and the first high-precision O isotope data for IIAB iron meteorites. The new data demonstrate that IIG iron meteorites belong to the non-carbonaceous (NC) meteorites. This is evident from the isotope anomaly of each of the four elements investigated, where the IIG irons always overlap with the compositions of NC meteorites but are distinct from those of carbonaceous (CC) meteorites. Moreover, among the NC meteorites and in particular, the NC irons, the isotopic composition of the IIG irons overlaps only with that of the IIAB irons. The combined Fe-Ni-O-Cr isotope data for IIAB and IIG iron meteorites, therefore, reveal formation from a single isotopic reservoir, indicating a strong genetic link between the two groups. The indistinguishable isotopic composition of the IIAB and IIG irons, combined with chemical evidence for the formation of IIG irons as late-stage liquids of the IIAB core, strongly suggests that both groups originate from the same core. The results underscore the strength of utilizing multiple elements and their isotopic compositions to establish genetic links among meteorites, rather than using a single element. They also highlight the significance of integrating multiple geochemical tracers and petrologic observations to accurately determine genetic relationships and the formation of meteorites within the same parent body.

1. Introduction

Magmatic iron meteorites are thought to derive from the metallic cores of differentiated planetesimals and, based on their chemical composition, are subdivided into several groups, that may represent distinct parent bodies (e.g., Scott and Wasson, 1975). In detail, magmatic irons that exhibit similar elemental fractionation trends (in logarithmic element-element diagrams) are chemically grouped into four categories, each designated by a Roman Numeral (i.e., I to IV) based on the abundances of moderately volatile siderophile elements, in particular Ga and Ge (Goldberg et al., 1951; Lovering et al., 1957). These categories are further subdivided into lettered groups based on Ga, Ge, Ni, and Ir concentrations (Wasson, 1967; Wasson and Kimbeblin, 1967), resulting in the eleven currently known groups of magmatic irons (not counting the non-magmatic groups IAB and IIE) (e.g., Goldstein et al., 2009). Two of these groups are IIAB and IIG, which while having similar Ga and Ge concentrations, are otherwise chemically distinct and have vastly different numbers of individual members (Wasson and Choe, 2009). Whereas group IIAB is the second largest magmatic group with more than 140 members, group IIG has only six members (Auburn, Bellsbank, Guanaco, La Primitiva, Tombigbee River, Twannberg), which is just above the minimum number of samples necessary to define an iron meteorite group (Wasson, 1974). Despite their chemical differences, an origin of both IIAB and IIG irons from two immiscible liquids in the same core has been proposed (Wasson and Choe, 2009).

Fractional crystallization models suggests that the IIAB core had

* Corresponding author at: Max Planck Institute for Solar System Research, Göttingen 37077, Germany.
E-mail address: anand@mps.mpg.de (A. Anand).

https://doi.org/10.1016/j.gca.2024.07.025
Received 18 April 2024; Accepted 22 July 2024
Available online 26 July 2024

relatively high concentrations of S (15–17 wt%) (Chabot, 2004; Zhang et al., 2024), P (0.1–1 wt%) (Jones and Drake, 1983; Zhang et al., 2024), and other volatile siderophile elements. This is evident from (1) a high abundance of trapped sulfide melt in evolved IIAB irons, (2) high concentrations of Ga and Ge relative to other magmatic iron groups, and (3) a steeply negative trend in the log-Ir vs. log-Au diagram (Wasson et al., 2007; Chabot, 2004; Hilton et al., 2022). Based on the high inferred S and P concentrations of the IIAB core, Wasson et al. (2007) proposed that during the later stages of crystallization, a buoyant immiscible S-rich liquid rose to the top of the S-poor core, ultimately resulting in complete separation of an upper S-rich and a lower P-rich (and S-poor) melt within the core. On this basis, Wasson and Choe (2009) suggested that the IIG iron meteorites, which are characterized by low S contents but the highest known bulk P contents among iron meteorites, sample the P-rich magma of the late-stage IIAB core. In this model, the characteristic high abundance of schreibersite in IIG iron meteorites is the result of entrapment of melt with relatively high P contents. The apparent association of IIAB and IIG iron meteorites is corroborated in element-Au diagrams where all IIG irons are typically located close to the high-Au end of the IIAB trend, beyond the compositions of late-crystallized IIAB irons (Wasson and Choe, 2009). Nevertheless, more quantitative modelling attempts aimed at matching the composition of solid IIG metal to the composition of late-stage IIAB irons have not been successful (Chabot et al., 2020).

A more direct link between IIAB and IIG iron meteorites can be established by measurements of their isotope compositions. For instance, O isotopes have widely been used to identify genetic links among and between meteorites, such as, between IAB irons and winonaites (Clayton and Mayeda, 1996; Greenwood et al., 2017), IIIAB irons and main-group pallasites (Clayton and Mayeda, 1996), IIE irons and H ordinary chondrites (Clayton et al., 1983; McDermott et al., 2016), and IVA irons and L or LL ordinary chondrites (Clayton et al., 1983). However, since O-bearing phases (i.e., chromites, phosphates, and silicates) are quite rare or even absent in the majority of iron meteorites, O isotope data for iron meteorites are scarce. In particular, no high-precision O isotope data are available for the IIAB and IIG irons that can be used to confirm or refute the IIAB-IIG relationship.

Over the last decade, a large-scale isotopic dichotomy between non-carbonaceous (NC) and carbonaceous (CC) meteorites has been identified (Warren, 2011; Budde et al., 2016; Kruijer et al., 2017). This NC-CC dichotomy has been revealed on the basis of using nucleosynthetic isotope anomalies in meteorites, which reflect the heterogeneous distribution of isotopically anomalous presolar components derived from several stellar nucleosynthetic sources (see Bermingham et al., 2020; Kleine et al., 2020; Kruijer et al., 2020 for some recent reviews). Since these anomalies do not result from mass-dependent isotope fractionation, they are not modified by parent body processes such as differentiation, fractional crystallization, or volatile depletion, and hence are powerful tools for identifying potential genetic links among and between different classes and groups of meteorites. Of the elements showing nucleosynthetic isotope variability, the siderophile elements Mo (e.g., Dauphas et al., 2002; Burkhardt et al., 2011; Worsham et al., 2017), Ru (Chen et al., 2010; Fischer-Gödde et al., 2015; Worsham et al., 2019), Ni (Regelous et al., 2008; Steele et al., 2011; Nanne et al., 2019), and Fe (Schiller et al., 2020; Cook et al., 2021; Hopp et al., 2022a) have most extensively been used for assessing genetic links among iron meteorites. However, although the strong chemical link between IIAB and IIG irons suggests that group IIG belongs to meteorites of the NC-type, this has yet not been demonstrated through isotope measurements. Genetic links between iron meteorites may also be evaluated using Cr isotopes, which show widespread ^{54}Cr anomalies among meteorites (Trinquier et al., 2007; Yamakawa et al., 2010; Qin et al., 2010; Zhu et al., 2020). This large variability combined with the current analytical uncertainty on ^{54}Cr measurements allows inter-group resolutions for almost all of the meteorite groups. In addition, the combined ε^{54}Cr-Δ^{17}O two-dimensional approach has proven very valuable for identifying genetic links among different meteorite groups (Warren, 2011). Chromium isotope variations in iron meteorites predominantly reflect spallation on Fe during cosmic ray exposure (CRE) (Qin et al., 2010). Consequently, nucleosynthetic ^{54}Cr signatures in iron meteorites can only be reliably determined if minerals with low Fe/Cr ratios, such as chromites, are available (Anand et al., 2021). However, chromites are extremely rare in iron meteorites. Therefore, similar to O isotopes, only a small number of iron meteorites have been studied for their primary Cr isotope compositions unaffected by spallogenic contributions (Anand et al., 2021).

In this study, new Fe, Ni, Cr, and O isotope data for group IIAB and IIG iron meteorites are used to determine whether the IIG irons are of the NC-type and to reassess the potential IIAB-IIG genetic relationship. The isotopic variations for Fe and Ni, in particular, are relatively small; therefore, it is difficult to distinguish among NC iron groups using only these elements. This problem is overcome by combining isotope data for four elements. When any of these elements are plotted against each other, the NC-CC dichotomy and the resolved isotopic variations among NC meteorites become visible. This makes it possible to unequivocally determine whether the IIAB and IIG irons share a common isotopic composition distinct from other iron meteorites and, hence, may derive from a common planetesimal core.

2. Samples and analytical methods

2.1. Samples and sample preparation

The isotope compositions of the samples were determined on either separated mineral phases (O, Cr) or bulk meteorite samples (Fe, Ni). Iron and Ni isotope compositions were determined for three IIG iron meteorites (Bellsbank [NHM London BM.1961,403], La Primitiva [NHM London BM.1927,77], Tombigee River [NHM London BM.84646]). Additionally, Ni isotope compositions were determined for six IIAB iron meteorites (Ainsworth, Braunau, Coahuila, Mt. Joy, North Chile, Sikhote Alin), one IC iron meteorite (Chihuahua City), and one IIIAB iron meteorite (Cape York) that were previously analyzed for their Fe, Mo, and Pt isotope compositions (Hopp et al., 2022a; Spitzer et al., 2020). For these analyses, ~600 mg of sample material each was digested in 6 M HCl (+trace conc. HNO_3) on a hotplate set to 130 °C for at least 24 h. Aliquots of these digestions corresponding to ~1000–2000 μg Fe and 40–100 μg Ni were processed through purification chemistry to obtain pure separates.

Chromite and/or troilite fractions were obtained each from Sikhote Alin (IIAB), Agoudal, Cape York (IIIAB; Agpalilik mass), and Twannberg (IIG) iron meteorites, from the Natural History Museum Bern (NMBE) collection (see Table 3 for collection numbers) and from two independent samples of Sikhote Alin from the Vernadski Museum, Moscow and from NMBE. Examination of many slabs of Twannberg revealed a single inclusion of chromite associated with the phosphate maricite. Chromite inclusions in the samples were first identified using an optical microscope and isolated as small fragments with attached metal-sulphide matrix. These fragments were digested in aqua regia on a hotplate set to 90 °C for 48 h to completely dissolve the matrix, leaving behind residual chromite grains. Troilite inclusions were separated from the iron meteorites using a Dremel® micro drill and were digested completely in aqua regia on a hot plate set to 90 °C for 48 h.

A fraction of the chromite extracted each from Sikhote Alin and Agoudal, and all of the recovered chromite fraction from Twannberg were used for O isotope analysis. Chromite fractions from Sikhote Alin, Agoudal and Cape York, and troilite fractions from Twannberg and Cape York were used to measure Cr isotopes. Of these, the Cr isotope data for the chromite fractions were previously reported in Anand et al. (2021), while the troilite fractions were analyzed as part of this study.

2.2. Chemical separation and purification

Iron was separated following the procedure described in Tang and Dauphas (2012) and Hopp et al. (2022a, 2022b). The sample aliquots were loaded in 0.25 ml 10 M HCl onto 10.5 cm long PFA columns filled with 3 ml pre-cleaned anion resin (AG1-X8, 200–400 mesh). Iron was retained on the resin while Ni and other major elements were eluted in 5 ml 10 M HCl. Other possible contaminants such as Cr were washed off using 30 ml 4 M HCl. Iron was eluted using 9 ml 0.4 M HCl, dried down, and re-dissolved in 10 M HCl for repetition of the procedure. The final purified Fe eluates were dried down and dissolved in 0.3 M HNO_3 for isotope measurements. The total procedural blank relative to the total Fe processed is negligible (~70 ng) and the overall Fe yields were >99 %. The interfering elements Cr (^{54}Cr on ^{54}Fe) and Ni (^{58}Ni on ^{58}Fe) were present at low levels (Cr/Fe $\leq 1.7 \times 10^{-6}$ and Ni/Fe $\leq 2 \times 10^{-6}$) which allow accurate Fe isotope ratio measurements.

The chemical separation of Ni involves a 3-step ion-exchange chromatography following the protocols described in Nanne et al. (2019), which are based on the method of Chernonozhkin et al. (2015). Sample solutions were loaded in 10 ml of 0.6 M HCl–90 % acetone onto PFA columns filled with 2 ml pre-cleaned and conditioned BioRad AG 50WX4 cation exchange resin (200–400 mesh). Most of the sample matrix (e.g., Fe, Cr) was eluted with an additional 35 ml 0.6 M HCl–90 % acetone and 10 ml 0.6 M HCl–95 % acetone before Ni was collected in 6 ml 0.6 M HCl–95 % acetone–0.1 M dimethylglyoxime (DMG). The second and third columns use BioRad AG1 X8 resin (100–200 mesh) and AG MP-1 X4 (100–200 mesh) anion exchange resins, respectively, to remove the remaining interfering elements (Ti, Fe, and Zn). The final purified Ni eluates were dried down and dissolved in 0.3 M HNO_3 for isotope measurements. The total procedural blank relative to the total Ni processed is negligible (<10 ng) and the overall Ni yields were ~80 %. The interfering elements Fe (^{58}Fe on ^{58}Ni) and Zn (^{64}Zn on ^{64}Ni) were present at sufficiently low levels which allowed accurate Ni isotope ratio measurements (Render et al., 2018; Nanne et al., 2019).

The procedure for Cr separation involves a 3-step ion-exchange chromatography modified after Schoenberg and von Blanckenburg (2005), Trinquier et al. (2008a), and Yamakawa et al. (2009). The sample aliquots were loaded in 1 ml 6 M HCl onto 7.5 mL PFA columns filled with 2 ml pre-cleaned anion resin (AG1-X8, 100–200 mesh). The Cr eluates from the first columns were dried down, re-equilibrated, and loaded onto second columns filled with 2 ml cation resin (AG 50 W-X8 200–400 mesh). The second column produced a solution with mostly Cr but incompletely separated from Ti and V. The Cr eluates from the second columns were dried down, transformed into nitrate form and loaded onto third columns containing 0.5 ml cation resin (AG 50 W-X8 200–400 mesh) to obtain pure Cr separates, free of Ti and V. The total procedural blank relative to the total Cr processed is negligible (~20 ng) and the overall Cr yields were >80 %.

2.3. Isotopic analyses

Oxygen isotopes were analysed on a MAT 253 dual inlet mass spectrometer at the Open University following the protocol given in Greenwood et al. (2017).

Iron isotope measurements were performed at the University of Chicago on a Thermo Scientific Neptune MC-ICP-MS. Ion beams of ^{54}Fe, ^{56}Fe, ^{57}Fe, and ^{58}Fe were measured in static mode on Faraday collectors using a $10^{10}\Omega$ amplifier for ^{56}Fe and $10^{11}\Omega$ amplifiers for the other Fe isotopes. Possible isobaric interferences from ^{54}Cr and ^{58}Ni were measured simultaneously by monitoring ^{53}Cr and ^{60}Ni using Faraday cups connected to $10^{12}\Omega$ amplifiers. The measurements were made on the flat-topped peak shoulder in medium-resolution (MR) mode to resolve interferences from argide ions. The purified Fe solutions (10 μg/g in 0.3 M HNO_3) were introduced into the MC-ICP-MS at an uptake rate of ~100 μl/min using a cyclonic glass spray chamber and Pt sampler and H skimmer cones. Typical $^{56}Fe^{+}$ ion signal intensities were ~140 V (10^{10} Ω resistor). Sample and standard measurements consisted of 50 cycles of 8.369 s each and sample analyses were bracketed by measurements of the reference material IRMM-524a. On peak zero intensities were measured at the beginning of each sequence using the same acid solution used for the sample and standard solutions and were subtracted from all individual measurements. Instrumental and natural mass fractionation was corrected by internal normalization to $^{57}Fe/^{56}Fe = 0.023095$ using the exponential law (Dauphas and Schauble, 2016). All data are reported in the μ-notation, i.e., the parts-per-million deviation of the internally normalized ratios relative to the mean value of the IRMM-524A solution standards that were analyzed bracketing the sample measurements. The reported μ-values represent the mean of pooled solution replicates (N = 10–25), and uncertainties are reported as 2 standard errors (2 s.e.). Additionally, mass-dependent isotopic variations are monitored, which allow to monitor possible spurious effects on internally normalized isotope ratios introduced by natural mass fractionation (Tang and Dauphas, 2012).

Nickel isotope measurements were performed at the Institut für Planetologie, University of Münster on a Thermo Scientific Neptune Plus MC-ICP-MS using the established measurement protocols described in earlier studies from this laboratory (Nanne et al., 2019; Spitzer et al., 2022). Ion beams of ^{58}Ni, ^{60}Ni, ^{61}Ni, ^{62}Ni, and ^{64}Ni were analyzed in static mode on Faraday collectors using a $10^{10}\Omega$ amplifier for ^{58}Ni and $10^{11}\Omega$ amplifiers for the other Ni isotopes. Measurements were made on a flat top section of the left-peak shoulder using MR mode to avoid possible interferences on mass ^{57}Fe from $^{40}Ar^{16}OH$ or $^{40}Ar^{17}O$ and $^{132}Xe^{2+}$ on ^{66}Zn (Makhatadze et al., 2023; Tang and Dauphas, 2012). The purified Ni solutions (1–2 μg/g in 0.3 M HNO_3) were introduced into the MC-ICP-MS at an uptake rate of ~50 μl/min using a Aridus II desolvator and standard sampler and X skimmer cones. Typical $^{58}Ni^{+}$ ion signal intensities were ~100 V (10^{10} Ω resistor). Sample and standard measurements consisted of 50 cycles of 8.4 s integrations each and sample analyses were bracketed by measurements of the reference material SRM 986. Prior to each sample or standard measurement, baselines were measured as on peak zeros (OPZ) for 20 × 8.4 s using the same acid solution used for the sample and standard solutions. Instrumental and natural mass fractionation was corrected by internal normalization to either $^{61}Ni/^{58}Ni = 0.016744$ or $^{62}Ni/^{61}Ni = 3.1884$ using the exponential law (Gramlich et al., 1989). All data are reported in the μ-notation relative to the mean value of the SRM 986 solution standards that were analyzed bracketing the sample measurements. The reported μ-values represent the mean of pooled solution replicates (N = 10–15) and uncertainties are reported as 2 s.e. The accuracy and precision of the isotope measurements were assessed by repeated analyses of the NIST 361 metal standard (Spitzer et al., 2022).

Chromium isotope measurements were performed at the Institute of Geological Sciences, University of Bern on a Thermo Scientific Triton Plus TIMS. Ion beams of ^{50}Cr, ^{51}V, ^{52}Cr, ^{53}Cr, ^{54}Cr, ^{55}Mn, and ^{56}Fe were analyzed in static mode on Faraday collectors using $10^{11}\Omega$ amplifiers (Trinquier et al., 2008a). Isobaric interferences of ^{54}Fe on ^{54}Cr were corrected by measuring ^{56}Fe. The ^{51}V intensities were not resolved from background intensities for all samples, demonstrating the successful separation of V from Cr during column chromatography. Two to three μg of purified Cr was loaded onto each single filament and measured at a ^{52}Cr signal intensity between 7 and 10 V (10^{11} Ω resistor). A typical run for a single filament load consisted of 24 blocks with 20 cycles each (integration time = 8.389 s). Gain calibration was done once, at the beginning of every analytical session. The baseline was measured (30 cycles, each of 1.05 s), and the amplifiers were rotated after every block. The Cr standard reference material NIST SRM 979 was used as a terrestrial reference material. The $^{53}Cr/^{52}Cr$ and $^{54}Cr/^{52}Cr$ ratios were normalized to $^{52}Cr/^{50}Cr = 19.28323$ (Shields et al., 1966) by applying the exponential mass fractionation law. All data are reported in the ε-notation, i.e., the parts-per-ten-thousand deviation of the internally normalized ratios relative to the mean value of the standard reference material (NIST SRM 979) measured along with the samples in each

measurement session (single turret). The reported ε^{i}Cr for any sample represents the mean of the replicate measurements and the uncertainties reported as 2 s.e. The uncertainties (2 standard errors, n = 8) for the standard reference material (NIST SRM 979) in each measurement session was ~0.05 for ε^{53}Cr and ~0.11 for ε^{54}Cr.

The Cr, Mn, and Fe concentrations of troilite and chromite fractions were determined on digestion aliquots, taken before the Cr purification, using a 7700x Agilent ICP-MS at the Institute of Geography, University of Bern. Uncertainties on ^{55}Mn/^{52}Cr and Fe/Cr ratios are reported in 2 s.e. of the replicate measurements (n = 5) and remained <5 % for all the samples.

3. Results

The Fe isotope compositions of the IIG iron meteorites are given in Table 1 and shown in Fig. 1. All three samples have resolvable isotope anomalies in μ^{54}Fe relative to IRMM-524a, but no resolvable variations in μ^{58}Fe. The weighted averages for μ^{54}Fe and μ^{58}Fe are +13 ± 3 and −1 ± 7, respectively. The same samples display no significant mass-dependent variations in δ^{56}Fe relative to IRMM-524, indicating that any spurious effects on the internally normalized Fe isotope ratios can be excluded (Tang and Dauphas, 2012). As shown in Fig. 1, the measured μ^{54}Fe for IIAB irons except for Ainsworth (data from Hopp et al., 2022a) are indistinguishable from those of the IIG irons of this study but are shifted towards slightly negative μ^{58}Fe values (Fig. 1). As discussed by Hopp et al. (2022a), these small shifts reflect CRE (see below).

The Ni isotope data for the studied irons are reported in Table 2 and shown in Fig. 2. When normalized to ^{61}Ni/^{58}Ni all samples display negative μ^{60}Ni, μ^{62}Ni, and μ^{64}Ni values, which is the characteristic composition of NC meteorites. The new Ni isotope data for Chihuahua City (IC), Cape York (IIIAB), and the analyzed IIAB irons agree with previously published values for samples from these groups of meteorites (Regelous et al., 2008; Steele et al., 2011; Tang and Dauphas, 2012; Nanne et al., 2019). There are no resolved Ni isotope variations among the six IIAB irons analyzed in this study, although these samples are characterized by very different CRE times and associated secondary neutron capture effects, as is evident from their variable Pt isotope anomalies (Table 2). The three IIG irons of this study also have indistinguishable Ni isotope compositions with mean μ^{60}Ni, μ^{62}Ni, and μ^{64}Ni values of −4±2, −13±5, and −39±8, respectively (Table 2). These values are identical to the mean values for the IIAB irons but are distinct from all other NC irons such as the IC irons (Table 2).

The new Cr isotope data for troilite from Twannberg and Cape York alongside data for chromite and daubréelite for IIAB and IIIAB irons from Anand et al. (2021) are listed in Table 3 and plotted in Fig. 3. The Fe/Cr and ^{55}Mn/^{52}Cr of Cape York troilite agree within analytical uncertainties with the measurements of the 'evenly distributed troilite component' reported in Jochum et al. (1975). The Fe/Cr ratio of ~353 measured in Twannberg troilite is lower than the Fe/Cr of ~850 for the troilite fraction from Cape York. The high Cr content of Twannberg troilite might be due to daubréelite intergrowths within the sampled troilite. The Cape York troilite displays higher ε^{53}Cr and ε^{54}Cr compared to previously reported values for chromite from this iron meteorite (Anand et al., 2021), which are also higher than the values for chromites from IIAB irons reported in the same study. The troilite from Twannberg exhibits even higher ε^{53}Cr and ε^{54}Cr than the Cape York troilite. As will be shown below, these differences most likely reflect the effects of CRE.

The new O isotope data for chromites from the IIAB irons Sikhote-Alin and Agoudal, and the IIG iron Twannberg are given in Table 3 and plotted in Fig. 4. All three meteorites have similar Δ^{17}O compositions. Fig. 4 compares the Δ^{17}O data of IIAB and IIG irons with that of other iron meteorite groups that contain an O-bearing mineral. The Δ^{17}O of IIAB iron meteorites Sikhote-Alin and Agoudal is analytically indistinguishable from that of the Twannberg IIG meteorite and suggests a similar source reservoir in the solar nebula for both iron meteorite groups. The variations in δ^{17}O and δ^{18}O between different meteorites and within Sikhote Alin reflect possible mass dependent isotope fractionation.

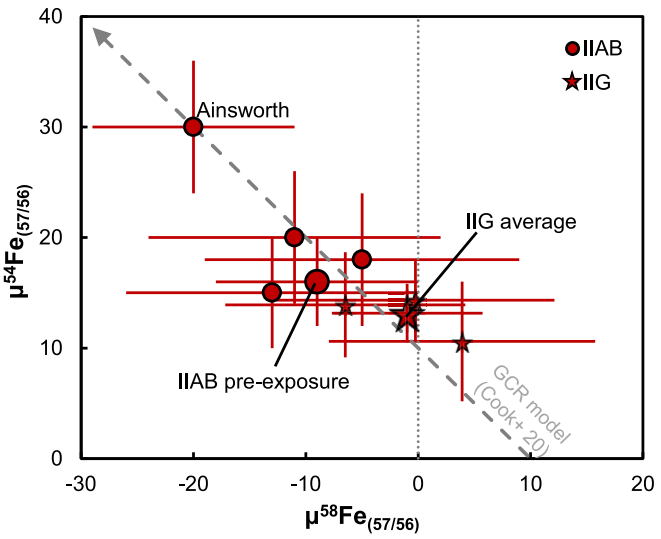

Fig. 1. Diagram of μ^{54}Fe and μ^{58}Fe in IIAB and IIG iron meteorites. The μ^{54}Fe and μ^{58}Fe compositions of the IIAB iron meteorite Ainsworth show significant effects from CRE and together with the other IIAB iron meteorites define a linear correlation between unirradiated and irradiated samples (Hopp et al. 2022a). The Fe isotope compositions of the three IIG iron meteorites do not show any intra-group variations in μ^{54}Fe and no resolvable μ^{58}Fe values. The weighted average of the IIG iron meteorites is within uncertainties similar to the pre-exposure values of the IIAB iron meteorite parent body. GCR model is from Cook et al. (2020).

Table 1
Fe isotope compositions of IIG iron meteorites.

Sample	N[a]	μ^{54}Fe[b]	2 s.e.[c]	μ^{58}Fe[b]	2 s.e.	δ^{56}Fe[d]	2 s.e.	Ref.
IIG iron meteorites								
Bellsbank	15	14	5	−6	11	0.04	0.02	ts.
La Primitiva	25	11	5	4	12	0.07	0.02	ts.
Tombigee River	10	14	4	0	12	0.03	0.02	ts.
Weighted Average		**13**	**3**	**−1**	**7**	**0.05**	**0.02**	
Pre-exposure IIAB		16	4	−9	9	–	–	a

References: (a) Hopp et al. (2022a). ts. = this study.
[a] Number of individual analyses.
[b] Fe isotopic composition internally normalized to ^{57}Fe/^{56}Fe = 0.023095 and expressed as μ-notation defined as the parts-per-million deviation of the ^{5x}Fe/^{56}Fe ratio in the sample relative to the two IRMM-524a standard solution bracketing measurements.
[c] Uncertainties were calculated using $\sigma t_{0.95}$, n − $1/\sqrt{n}$.
[d] Mass-dependent Fe isotope composition calculated by sample-standard bracketing and given as δ-notation defined parts-per-thousands deviation of the ^{56}Fe/^{54}Fe ratio of the sample relative to the IRMM-524a standard solution.

4. Discussion

4.1. Assessment of cosmogenic effects on the isotopic composition of IIG iron meteorites

In addition to nucleosynthetic variability, the isotope composition of meteorites may be modified by CRE. Nuclear reactions induced by the interactions of cosmic ray particles with target atoms produce new cosmogenic nuclides, resulting in isotopic variations superimposed on the original nucleosynthetic variability among meteorites. These effects can be particularly significant for iron meteorites, which typically have longer CRE times compared to most other meteorite groups. For

Table 2
Ni isotope compositions of iron meteorites analyzed in this study.

Sample	N	$\mu^{60}Ni_{(61/58)}$	2 s.e.	$\mu^{62}Ni_{(61/58)}$	2 s.e.	$\mu^{64}Ni_{(61/58)}$	2 s.e.	$\mu^{58}Ni_{(62/61)}$	2 s.e.	$\mu^{60}Ni_{(62/61)}$	2 s.e.	$\mu^{64}Ni_{(62/61)}$	2 s.e.	Ref.	$\varepsilon^{196}Pt$	95 % CI	Ref.
IIG irons																	
Bellsbank	15	−4	3	−14	8	−35	14	−42	24	−17	10	5	16	ts.	–	–	
La Primitiva	15	−4	4	−9	7	−37	12	−28	21	−13	10	−11	15	ts.	–	–	
Tombigee River	14	−6	4	−17	9	−53	18	−54	28	−24	13	−2	14	ts.	–	–	
Wt. Avg.		**−4**	**2**	**−13**	**5**	**−39**	**8**	**−39**	**13**	**−17**	**6**	**−3**	**8**				
IIAB irons																	
Ainsworth	12	−4	4	−19	8	−35	18	−28	24	−14	12	−8	18	ts.	1.09	0.06	a
Braunau	12	−7	5	−10	11	−40	21	−32	33	−17	15	−10	17	ts.	−0.03	0.06	a
Mt Joy	11	−5	6	−16	4	−41	13	−48	14	−21	8	5	12	ts.	0.26	0.04	a
North Chile	15	−2	3	−6	8	−41	9	−18	24	−8	11	−24	17	ts.	0.02	0.03	a
Sikhote-Alin	15	−6	5	−12	9	−49	16	−39	27	−18	13	−12	20	ts.	0.32	0.09	a
Coahuila		−4	1	−9	9	−29	24	−29	28	−13	8	−2	3	b, c	–	–	
Wt. Avg.		**−4**	**1**	**−12**	**3**	**−41**	**6**	**−37**	**9**	**−15**	**4**	**−3**	**3**				
IC irons																	
Chihuahua City	15	−4	2	−11	4	−35	10	−35	14	−16	6	−1	8	ts.	0.09	0.07	a
Wt. Avg.		**−5**	**1**	**−4**	**3**	**−18**	**7**	**−12**	**9**	**−10**	**4**	**−5**	**4**				
IIIAB irons																	
Cape York	14	−4	3	−10	6	−26	12	−30	19	−14	9	3	13	ts.	0.01	0.04	a
Wt. Avg.		**−5**	**2**	**−11**	**2**	**−32**	**7**	**−41**	**4**	**−18**	**3**	**0**	**6**				

References: (a) Spitzer et al. (2020), (b) Tang and Dauphas (2012), (c) Steele et al. (2011), ts. = this study.
The weighted average for IC and IIIAB irons includes literature data from Nanne et al. (2019), Steele et al. (2011), and Tang and Dauphas (2012).

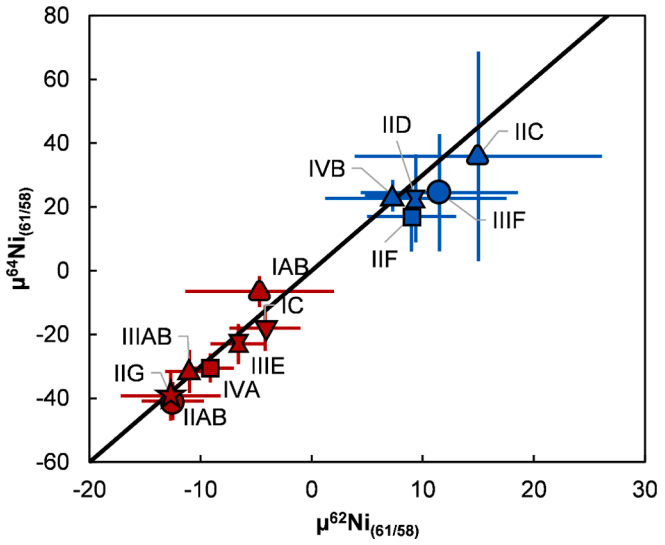

Fig. 2. $\mu^{64}Ni_{(61/58)}$ vs. $\mu^{62}Ni_{(61/58)}$ compositions for the major iron meteorite groups. Samples plot along a line with a slope of ~3 (Steele et al., 2011; Nanne et al., 2019). Data are from this study and compiled from the literature (Steele et al., 2011; Tang and Dauphas, 2012, Cook et al., 2020; Nanne et al., 2019; Cook et al., 2021).

instance, significant CRE effects on the isotope compositions of the siderophile elements W (e.g., Kruijer et al., 2012), Mo (e.g., Worsham et al., 2017; Spitzer et al., 2020), Pt (e.g., Kruijer et al., 2013; Wittig et al., 2013), and Os (e.g., Walker, 2012) have been shown to predominantly reflect secondary neutron capture reactions. Recent model calculations for Fe and Ni have shown that potential CRE-induced isotope shifts in these two elements are also dominated by secondary neutron capture reactions (Cook et al., 2020). By contrast, Cr CRE-induced effects in iron meteorites are predominantly caused by spallation reactions on Fe (e.g., Qin et al., 2010). Given this evidence for ubiquitous CRE effects in iron meteorites, it is important to assess any such effects on the Fe-Ni-Cr isotope compositions of the IIAB and IIG irons of this study before these data are interpreted in terms of potential genetic links among these samples.

Cook et al. (2020) showed that while CRE effects on Fe isotopes in iron meteorites are expected to be small, they may be significant for samples with extremely long CRE. This is consistent with observations of Hopp et al. (2022a), who found resolvable CRE effects on Fe isotopes in IIAB irons, which compared to the pre-exposure composition resulted in higher $\mu^{54}Fe$ and lower $\mu^{58}Fe$ values (Fig. 1). These authors also showed that the CRE effects on Fe isotopes can be corrected using Pt isotopes measured as an in-situ neutron dosimeter in the same samples (Hopp et al., 2022a). However, Hopp et al. (2022a, 2022b) also showed that within current analytical precision, meteorites display no nucleosynthetic anomalies for $\mu^{58}Fe$; therefore, CRE-induced shifts in $\mu^{54}Fe$ can be corrected using the measured $\mu^{58}Fe$ of a sample together with the $\mu^{54}Fe$-$\mu^{58}Fe$ slope observed for CRE-induced shifts. The three IIG irons of this study do not show any variations in $\mu^{54}Fe$ and have no anomaly on $\mu^{58}Fe$ (Fig. 1), indicating that CRE-effects on Fe isotopes are absent for these samples. The mean Fe isotope composition of these samples is, therefore, representative of the composition of the IIG irons.

For Ni isotopes, prior studies have shown that the absolute magnitude of CRE effects is minimal and smaller than the current analytical precision of the Ni isotope measurements (Cook et al., 2020; Nanne et al., 2019). This is supported by the new Ni isotope data for IIAB irons presented here, which include data for Ainsworth, one of the most strongly irradiated irons. When combining the Ni isotope data presented here with previously published Pt isotope compositions for the same samples (Spitzer et al., 2020) no significant variations outside the analytical uncertainties is observed, which is consistent with model predictions (Fig. 5). Thus, no CRE-correction is needed for the IIG samples of this study and their weighted mean Ni isotopic composition is representative for the composition of the IIG iron meteorite parent body.

For Cr isotopes the situation is more complicated, as cosmogenic Cr can be produced by spallation of Fe, Ni, and Cr, and by neutron capture of Cr itself. For iron meteorites, spallation on Fe is the dominant source of cosmogenic Cr, where the amount of cosmogenic Cr produced depends on (1) CRE duration, (2) Fe/Cr ratio, and (3) the shielding of a sample (Birck and Allegre, 1985; Shima and Honda, 1966; Liu et al.,

Table 3
Cr and O isotope compositions, Fe/Cr ratios, and CRE ages of IIAB and IIG iron meteorites.

Sample	CRE age (Ma)	Mineral	$^{55}Mn/^{52}Cr$	Fe/Cr	$\delta^{18}O$	2 s.e.	$\delta^{17}O$	2 s.e.	$\Delta^{17}O$	2 s.e.	Ref.	$\varepsilon^{53}Cr$	2 s.e.	$\varepsilon^{54}Cr$	2 s.e.	Ref.
IIAB iron meteorites																
Sikhote-Alin (NMBE 43380)		Chromite	0.005	0.41	−2.05		−2.23		−1.16		ts.	−0.23	0.03	−0.92	0.05	a
Sikhote-Alin (Vernadski 1821)		Chromite			0.53	0.08	−0.88	0.05	−1.16	0.01	ts.					
Agoudal (NMBE 43830)		Chromite	0.005	0.37	0.64		−0.85		−1.18		ts.	−0.21	0.02	−0.78	0.06	a
NWA 11,420 (NMBE 43837)		Daubréelite	0.004	0.59	–		–		–			−0.20	0.05	−0.77	0.06	a
Average									**−1.17**	**0.03**		**−0.21**	**0.03**	**−0.83**	**0.17**	**a**
IIG iron meteorites																
Twannberg (TW342)	193 ± 43	Chromite			−0.69		−1.46		−1.10		ts.					a
Twannberg (TW1)	193 ± 43	Troilite	0.148	352	–		–		–			0.01	0.02	−0.31	0.04	ts.
Pre-exposure Twannberg					–		–		–			−0.22	0.06	−0.90	0.15	ts.
IIIAB iron meteorites																
Cape York (NMBE 33137)	82 ± 7	Chromite	0.006	0.46	2.03		0.77		−0.30		b	−0.20	0.04	−0.78	0.06	a
Cape York (NMBE 33137)	82 ± 7	Troilite	0.170	850	–		–		–			−0.07	0.04	−0.46	0.09	ts.

References: (a) Anand et al. (2021), (b) Clayton and Mayeda (1996). References for CRE ages: Twannberg (Smith et al., 2019), Cape York (Mathew and Marti, 2009), ts. = this study.
The reproducibility of $^{55}Mn/^{52}Cr$ and Fe/Cr ratios is better than 5%. The pre-exposure $\varepsilon^{53}Cr$ and $\varepsilon^{54}Cr$ abundances represent the spallogenic Cr-corrected Twannberg troilite data (and propagated uncertainties).

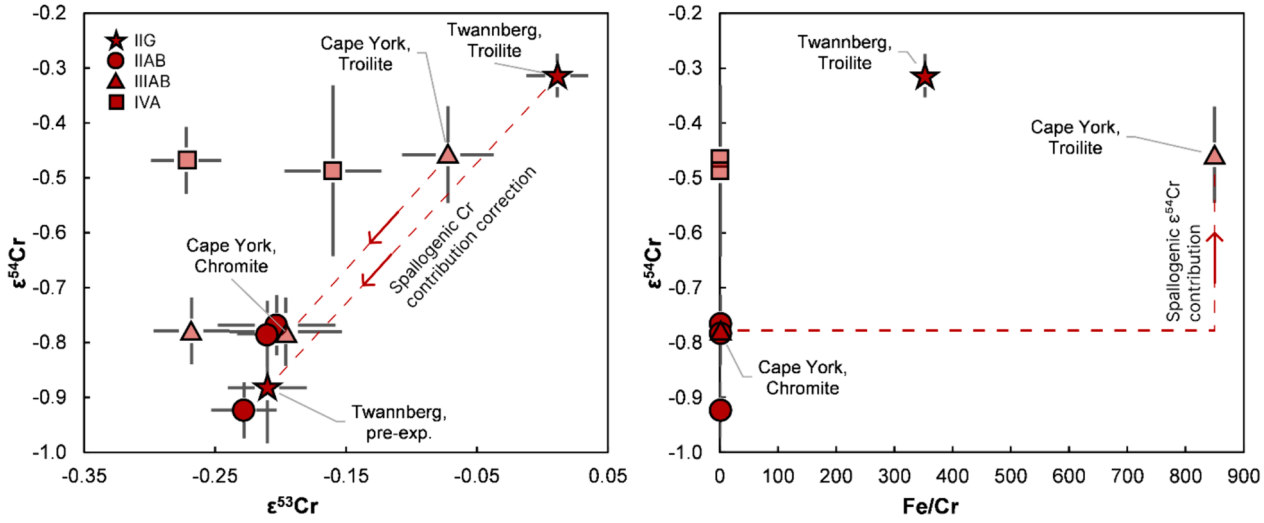

Fig. 3. (a) $\varepsilon^{54}Cr$ vs. $\varepsilon^{53}Cr$ and (b) $\varepsilon^{54}Cr$ vs. Fe/Cr plots for the iron meteorite chromite/daubréelite/troilite fractions. The dashed lines in (a) show spallogenic Cr contribution correction for the troilite fractions. The pre-exposure $\varepsilon^{54}Cr$ of Twannberg iron meteorite is determined assuming the same pre-exposure $\varepsilon^{53}Cr$ compositions of IIAB and IIG iron meteorites and a slope of ~2.6 for the coupled $\varepsilon^{53}Cr$ and $\varepsilon^{54}Cr$ spallogenic excesses given by Cape York troilite-chromite pair. Error bars represent 2 s.e. uncertainties.

2019). Thus, unlike the other aforementioned elements, CRE effects on Cr isotopes also depend on the chemical composition of samples and as such cannot easily be corrected using an *in-situ* monitor for these effects. In particular, the metal phase of iron meteorites cannot be used to reliably determine nucleosynthetic Cr isotope signatures because the high Fe/Cr ratios (≥100,000) lead to significantly elevated spallogenic coupled ^{53}Cr and ^{54}Cr excesses on the order of 100 s of ε-units with a best-fit line of $\varepsilon^{54}Cr = (3.90 \pm 0.03) \times \varepsilon^{53}Cr$ (e.g., Liu et al., 2019). The correlated nature of the CRE-induced $\varepsilon^{53}Cr$ and $\varepsilon^{54}Cr$ excesses potentially allows for the correction of these effects if the pre-exposure values of either $\varepsilon^{53}Cr$ or $\varepsilon^{54}Cr$ are known. However, the $\varepsilon^{53}Cr$–$\varepsilon^{54}Cr$ slope of the CRE-induced variations depends on the sample matrix, and modelling yields a slightly shallower slope of 3.6 ± 0.2 for metal and a higher slope of ~5.4 for olivine in stony meteorites (Liu et al., 2019). Moreover, Mougel et al. (2018) reported a much shallower slope of ~2.62 for lunar samples, and these authors argued that secondary neutron capture reactions rather than spallation are responsible for the CRE effects on Cr isotopes in lunar samples.

In contrast to metal, chromite and daubréelite inclusions in iron meteorites have low Fe/Cr ratios (~0.5), thus cosmogenic contributions of Fe spallation to ^{53}Cr and ^{54}Cr are minor to absent (Trinquier et al., 2008b; Liu et al., 2019). Consequently, the pre-exposure Cr isotopic compositions of iron meteorites are best determined on chromite or daubréelite inclusions from these samples (Anand et al., 2021). However, chromite and daubréelite are both extremely rare in iron meteorites. In their absence, troilite, which is another substantial Cr carrier phase, is the second-best choice for determining pre-exposure Cr isotope compositions, but given its elevated Fe/Cr of ~500, correction for CRE effects is required. For this correction, the Cr isotope data for chromite (Anand et al., 2021) and troilite (this study) from the IIIAB iron meteorite Cape York were used. The CRE effect on Cr isotopes can be approximated by (Qin et al., 2010):

$$\varepsilon^{i}Cr^{*} \propto A \times (Fe/Cr) \times 1/f(d) \quad (1)$$

where $\varepsilon^{i}Cr^{*}$ is the change due to CRE effects, A is the CRE age of a

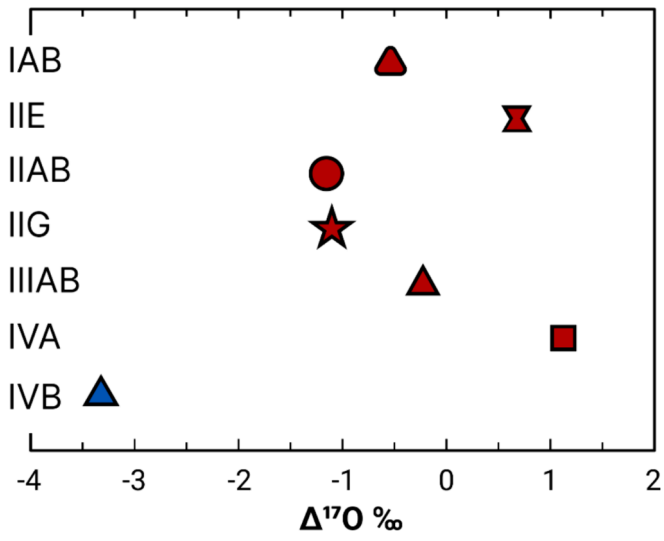

Fig. 4. $\Delta^{17}O$ compositions of IIAB iron meteorites Sikhote-Alin and Agoudal, and IIG iron meteorite Twannberg investigated in the present study and other iron meteorites groups from the literature (Clayton and Mayeda, 1996; Wang et al., 2004; McDermott et al., 2016; Corrigan et al., 2022). Error bars are smaller than the data points.

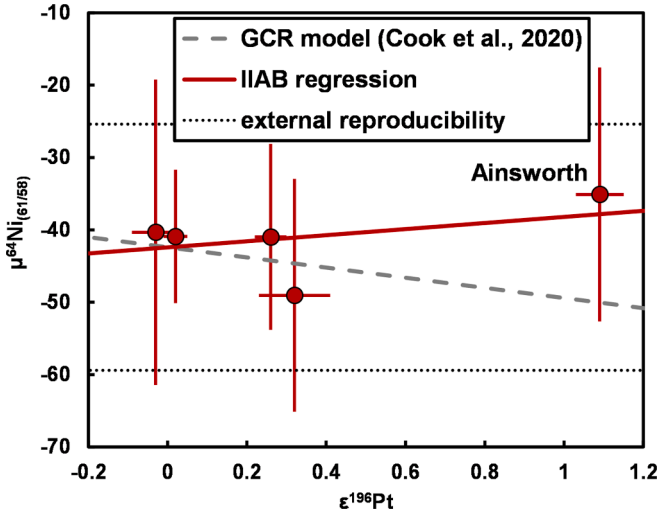

Fig. 5. Diagram of $\mu^{64}Ni_{(61/58)}$ vs. $\varepsilon^{196}Pt$ for IIAB iron meteorites illustrating that Ni isotope measurements of even highly irradiated samples like Ainsworth are not significantly affected by CRE effects within the current analytical precision. This agrees with theoretical models of CRE effects by Cook et al. (2020) and demonstrates that there is no need for correction.

sample, and $f(d)$ is the shielding factor, which is a function of the distance 'd' of a sample from the pre-atmospheric surface of the parent meteoroid. For each sample, $\varepsilon^{i}Cr^{*}$ can also be calculated as the difference in $\varepsilon^{i}Cr$ between troilite and chromite, because owing to their low Fe/Cr, the measured $\varepsilon^{i}Cr$ of chromites provides the pre-exposure value of a sample:

$$\varepsilon^{i}Cr_{0}^{*} = \varepsilon^{i}Cr_{troilite} - \varepsilon^{i}Cr_{chromite(pre-exposure)} \quad (2)$$

Combining and rearranging Eq. (1) and Eq. (2) for Twannberg and Cape York iron meteorites, yields:

$$\varepsilon^{i}Cr_{Twannberg}^{pre-exposure} = \varepsilon^{i}Cr_{Twannberg}^{Troilite} - \varepsilon^{i}Cr_{Cape\ York}^{*} \times \frac{A_{Twannberg} \times \left(\frac{Fe}{Cr}\right)_{Twannberg} \times f(d)_{Cape\ York}}{A_{Cape\ York} \times \left(\frac{Fe}{Cr}\right)_{Cape\ York} \times f(d)_{Twannberg}} \quad (3)$$

Using the $\varepsilon^{54}Cr$ and $\varepsilon^{53}Cr$ values and Fe/Cr ratios for troilite and chromite fractions and exposure ages for Cape York and Twannberg iron meteorites from Table 3 and assuming $\frac{f(d)_{Twannberg}}{f(d)_{Cape\ York}} = 1$, the pre-exposure Cr isotope composition of Twannberg is $\varepsilon^{53}Cr_{Twannberg} = -0.11 \pm 0.07$ and $\varepsilon^{54}Cr_{Twannberg} = -0.63 \pm 0.13$ (Fig. 3). However, if $\frac{f(d)_{Twannberg}}{f(d)_{Cape\ York}} > 1$, then $\varepsilon^{53}Cr_{Twannberg} > -0.11 \pm 0.07$ and $\varepsilon^{54}Cr_{Twannberg} > -0.63 \pm 0.13$. Similarly, if $\frac{f(d)_{Twannberg}}{f(d)_{Cape\ York}} < 1$ then, $\varepsilon^{53}Cr_{Twannberg} < -0.11 \pm 0.07$ and $\varepsilon^{54}Cr_{Twannberg} < -0.63 \pm 0.13$. Thus, since the shielding factors for the respective samples from Twannberg and Cape York are unknown, $\frac{f(d)_{Twannberg}}{f(d)_{Cape\ York}}$ cannot be quantified with certainty and the pre-exposure $\varepsilon^{i}Cr$ values of Twannberg cannot be determined precisely using this approach.

An alternative approach is to use the Cr isotope compositions of the Cape York troilite and chromite fractions to determine the slope of the coupled spallogenic $\varepsilon^{53}Cr$ and $\varepsilon^{54}Cr$ excesses in these low Fe/Cr samples. This yields a slope of ~2.6 which is lower than the slope of 3.9 determined for the much higher Fe/Cr metal phases in iron meteorites (Liu et al., 2019), but agrees with the slope of ~2.62 determined for lunar samples, which are also characterized by low Fe/Cr ratios (Mougel et al., 2018). This slope can be used to determine the pre-exposure Cr isotopic composition of Twannberg from the measured composition for troilite and by assuming a pre-exposure value for either $\varepsilon^{53}Cr$ or $\varepsilon^{54}Cr$. A prior study (Anand et al. 2021) has shown that the pre-exposure $\varepsilon^{53}Cr$ of magmatic iron meteorites, determined on chromite samples, reflect the time of Mn-Cr fractionation during core formation and that the $\varepsilon^{53}Cr$ values among the IIAB, IIIAB, and IVA irons vary only from −0.27 to −0.16. Assuming that the pre-exposure $\varepsilon^{53}Cr$ of Twannberg falls within this range of values and using a slope of ~2.6 (obtained from Cape York troilite-chromite pair) for the coupled spallogenic $\varepsilon^{53}Cr$ and $\varepsilon^{54}Cr$ excesses, the pre-exposure $\varepsilon^{54}Cr$ of Twannberg is -0.90 ± 0.15. This value agrees with the average $\varepsilon^{54}Cr = -0.83 \pm 0.17$ for the IIAB iron meteorites.

4.2. NC origin of IIG irons and a common parent body for IIG and IIAB iron meteorites

The Fe-Ni-O-Cr isotope data of this study provide two key observations. First, the IIG irons, as expected, are of the NC type. This is evident from the isotope anomalies of each of the four elements investigated, where the IIG irons in all cases overlap with the compositions of NC meteorites but are distinct from those of CC meteorites. This is also evident when either of these four elements is plotted against the other. In these plots, the IIG irons plot within, but close to one end of the NC field (Fig. 6). As such, the IIG iron meteorite group is not only the last of the iron meteorite groups for which the association to either the NC- or CC-type has been established, but together with IIAB iron meteorites and ureilites, they also define one endmember composition of the isotopic range among the NC meteorites. Second, among the NC meteorites and in particular NC irons the isotope compositions of the IIG irons overlaps only with that of the IIAB irons. This is not always clearly resolved for individual elements (in particular not for ^{54}Fe and ^{54}Cr), but is particularly evident when considering O isotopes. However, element-element plots of Fe, Ni, Cr, and O isotope anomalies show that for either element pair the IIG irons in all cases overlap with the composition of the IIAB irons and are distinct from all other meteorites. Thus, the combined Fe-Ni-O-Cr isotope data for IIAB and IIG iron meteorites unequivocally reveal the formation of their parent bodies in a common isotopic

reservoir, indicating a strong genetic link between the IIAB and IIG iron meteorites rather than a mere accidental association.

Although indistinguishable isotope compositions between meteorite groups can indicate an origin from a common isotopically distinct reservoir, determining whether these meteorite groups are derived from a common parent body also requires an evaluation of their petrologic and chemical similarities. There are a few examples of isotopic links between distinct meteorite groups, such as for the IAB irons and winonaites (Clayton and Mayeda, 1996; Greenwood et al., 2017), the IIIAB, IIIE irons and main-group pallasites (Scott et al, 1973; Clayton and Mayeda, 1996; Kruijer et al., 2022), the IIE irons and H chondrites (Clayton et al., 1983; McDermott et al., 2016), and the IVA irons and L/LL chondrites (Clayton et al., 1983). However, differences in petrology, chemical compositions, and formation times indicate that despite the isotopic links, all these meteorites formed in different parent bodies. For the IIAB and IIG irons this situation is different because, in addition to the strong isotopic link established in this study, these two groups of iron meteorites are also chemically linked. In particular, prior studies emphasized that the trace element composition of the IIG irons plot near the high-Au end (late-crystallized samples) of the IIAB field and on this basis argued that the IIG irons might be related to the late-stage metal liquid of the IIAB core after encountering liquid immiscibility (Wasson and Choe, 2009; Chabot et al., 2020). This combined with the new Fe-Ni-O-Cr isotope data of this study suggests strongly that the IIAB and IIG irons formed within the same asteroidal core.

The only other meteorite group with a similar isotope composition to the IIAB-IIG irons are the ureilites (Fig. 7). Although it is tempting to try to link silicate-dominated meteorites to the silicate mantle of iron meteorite parent bodies, such a link is not supported for the ureilites and IIAB-IIG irons. While the IIAB-IIG parent body formed within the first ~0.5–1 Ma of the solar system (Kruijer et al., 2014), the ureilite parent body probably formed only ~1 Ma later (Budde et al., 2015). The ureilite parent body remained incompletely differentiated (Collinet and Grove, 2020), while the IIAB-IIG iron meteorites sample the metallic core of a fully differentiated parent body (Wasson et al., 2007; Wasson and Choe, 2009). Moreover, ureilites contain significant amounts of carbon (~3 wt% on average) which is interpreted as a primary constituent of the ureilite parent material (Goodrich and Berkley, 1986). Due to its siderophile character, most of the C should differentiate into the core. However, IIAB iron meteorites are estimated to have derived from a relatively C-poor parent body (Grewal and Asimow, 2023). Finally, there is no evidence suggesting that the ureilite parent body was initially as P-rich as the IIAB-IIG parent body (Wasson et al., 2007; Wasson and Choe, 2009). These examples highlight that a strong isotopic link among differentiated meteorites does not imply formation within the same parent body, making the strong chemical and isotopic link between IIAB and IIG iron meteorites rather exceptional.

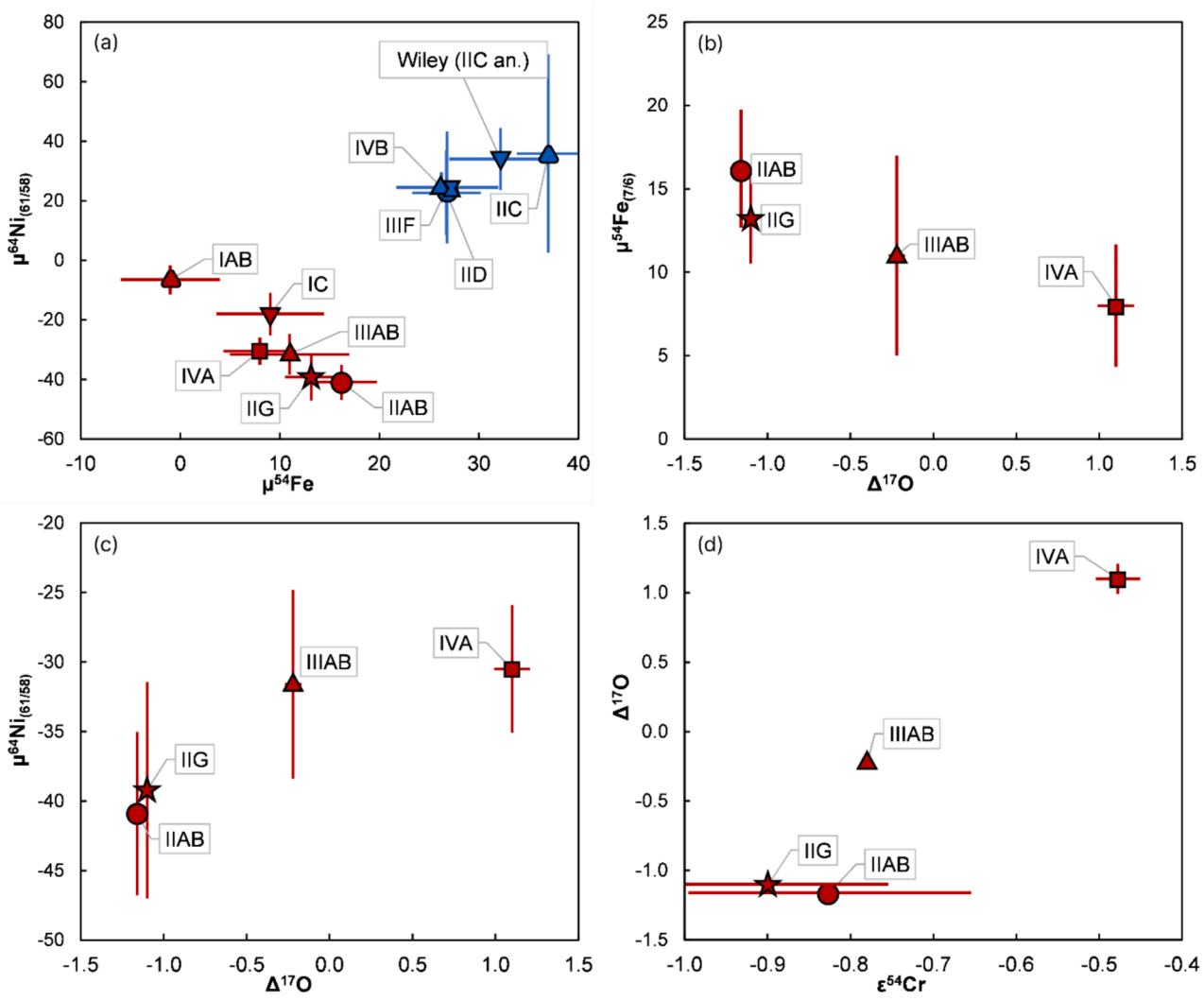

Fig. 6. (a)-(d) Oxygen, Cr, Fe, and Ni isotope compositions of different iron meteorite groups. The combined multi-isotope composition of IIAB and IIG iron meteorites show a clear overlap indicating that their parent bodies originated within the same isotopic reservoir.

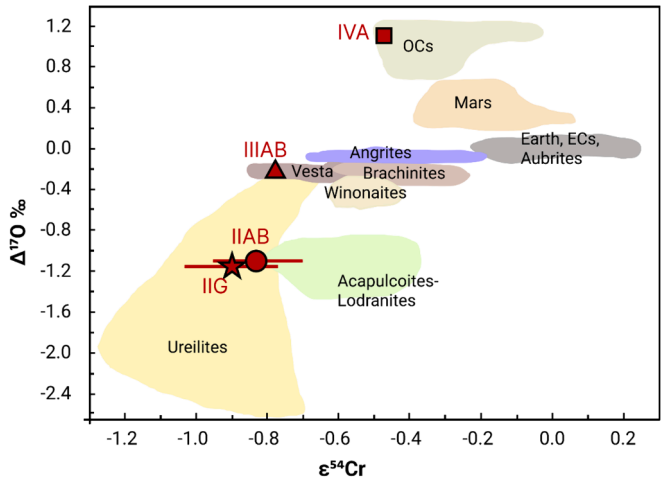

Fig. 7. Oxygen and Cr isotopic anomalies of non-carbonaceous iron meteorites, chondrites, and achondrites. Literature data are from Sanborn et al. (2019) and references therein.

5. Conclusions

This study reports the first Fe, Ni, O, and Cr isotope data for IIG iron meteorites as well as the first high-precision O isotope data for IIAB irons. The new data demonstrate that the IIG irons belong to the NC meteorites, making group IIG the last iron meteorite group for which the association to either the NC- or CC-type has been determined. The combined Fe-Ni-Cr-O isotope data demonstrate that group IIAB and IIG iron meteorites have identical isotopic compositions but are distinct from all other NC meteorites. This isotopic link underscores the strength of utilizing multiple elements to establish genetic links among meteorites, rather than using a single element. The identical isotope composition of the IIAB and IIG irons combined with chemical evidence for the formation of IIG irons as late-stage liquids of the IIAB core suggests strongly that the iron meteorites from both groups formed within the same planetesimal core. This highlights the significance of integrating multiple isotopic and geochemical tracers with petrologic observations to accurately determine genetic relationships and formation within the same parent body. This approach could prove particularly valuable for examining the substantial quantity of ungrouped iron meteorites (>100) to deepen the understanding of the origin and extent of nucleosynthetic variability in planetary materials, genetic relations of planetary bodies, the timing of planetary core formation in different disk regions, and the mixing processes within the solar accretion disk.

CRediT authorship contribution statement

Aryavart Anand: Writing – original draft, Visualization, Validation, Methodology, Investigation, Conceptualization. **Fridolin Spitzer:** Writing – review & editing, Visualization, Validation, Methodology, Investigation, Conceptualization. **Timo Hopp:** Writing – review & editing, Validation, Methodology, Investigation, Conceptualization. **Richard Windmill:** Methodology, Investigation. **Pascal Kruttasch:** Writing – review & editing, Validation. **Christoph Burkhardt:** Writing – review & editing, Validation. **Nicolas Dauphas:** Writing – review & editing, Validation, Conceptualization. **Richard Greenwood:** Methodology, Investigation. **Beda Hofmann:** Writing – review & editing, Resources, Methodology, Investigation, Conceptualization. **Klaus Mezger:** Writing – review & editing, Validation, Supervision, Resources, Conceptualization. **Thorsten Kleine:** Writing – review & editing, Validation, Supervision, Resources, Conceptualization.

Data availability

Data are available through Zenodo at https://doi.org/10.5281/zenodo.10985057.

Declaration of competing interest

The authors declare that they have no known competing financial interests or personal relationships that could have appeared to influence the work reported in this paper.

Acknowledgements

We thank Dmitrj Badyukov from the Vernasdski Institute, Moscow, for a sample of Sikhote Alin chromite. NHM London is thanked for providing the samples of Bellsbank, La Primavera, and Tombigbee River. Marc Jost discovered the chromite-phosphate inclusion in Twannberg mass 342 and donated it to NMBE for scientific investigation. A.A. and K. M. acknowledge the funding within the framework of the NCCR Planets supported by the Swiss National Science Foundation grant no. 51NF40182901 and 51NF40 205606 and "Swiss Government Excellence Scholarship (2018.0371)." N.D. was supported by NASA grants 80NSSC20K1409 (Habitable Worlds), 359NNX17AE86G (LARS), NNX17AE87G, and 80NSSC20K0821 (Emerging Worlds), EAR-2001098 (CSEDI), and a DOE grant. T.K. and C.B. were supported by the Deutsche Forschungsgemeinschaft (DFG, German Research Foundation) – Project-ID 263649064 – TRR 170. We express our gratitude to Audrey Bouvier for editorial handling, and to Joe Boesenberg and two anonymous reviewers for their constructive comments, which helped to improve the paper. This is TRR pub. No. 218.

References

Anand, A., Pape, J., Wille, M., Mezger, K., Hofmann, B.A., 2021. Early differentiation of magmatic iron meteorite parent bodies from Mn–Cr chronometry. Geochem. Perspect. Lett. 20, 6–10.
Bermingham, K.R., Füri, E., Lodders, K., Marty, B., 2020. The NC-CC isotope dichotomy: implications for the chemical and isotopic evolution of the early Solar System. Space Sci. Rev. 216, 1–29.
Birck, J.L., Allegre, C.J., 1985. Isotopes produced by galactic cosmic rays in iron meteorites. In: Isotopic Ratios in the Solar System, pp. 21–25.
Budde, G., Kruijer, T.S., Fischer-Gödde, M., Irving, A.J., Kleine, T., 2015. Planetesimal differentiation revealed by the Hf–W systematics of ureilites. Earth Planet. Sci. Lett. 430, 316–325.
Budde, G., Burkhardt, C., Brennecka, G.A., Fischer-Gödde, M., Kruijer, T.S., Kleine, T., 2016. Molybdenum isotopic evidence for the origin of chondrules and a distinct genetic heritage of carbonaceous and non-carbonaceous meteorites. Earth Planet. Sci. Lett. 454, 293–303.
Burkhardt, C., Kleine, T., Oberli, F., Pack, A., Bourdon, B., Wieler, R., 2011. Molybdenum isotope anomalies in meteorites: constraints on solar nebula evolution and origin of the Earth. Earth Planet. Sci. Lett. 312 (3–4), 390–400.
Chabot, N.L., 2004. Sulfur contents of the parental metallic cores of magmatic iron meteorites. Geochim. Cosmochim. Acta 68 (17), 3607–3618.
Chabot, N.L., Cueva, R.H., Beck, A.W., Ash, R.D., 2020. Experimental partitioning of trace elements into schreibersite with applications to IIG iron meteorites. Meteorit. Planet. Sci. 55 (4), 726–743.
Chen, J.H., Papanastassiou, D.A., Wasserburg, G.J., 2010. Ruthenium endemic isotope effects in chondrites and differentiated meteorites. Geochim. Cosmochim. Acta 74 (13), 3851–3862.
Chernonozhkin, S.M., Goderis, S., Lobo, L., Claeys, P., Vanhaecke, F., 2015. Development of an isolation procedure and MC-ICP-MS measurement protocol for the study of stable isotope ratio variations of nickel. J. Anal. At. Spectrom 30 (7), 1518–1530.
Clayton, R.N., Mayeda, T.K., Olsen, E.J., Prinz, M., 1983. Oxygen isotope relationships in iron meteorites. Earth Planet. Sci. Lett. 65 (2), 229–232.
Clayton, R.N., Mayeda, T.K., 1996. Oxygen isotope studies of achondrites. Geochim. Cosmochim. Acta 60 (11), 1999–2017.
Cook, D.L., Leya, I., Schönbächler, M., 2020. Galactic cosmic ray effects on iron and nickel isotopes in iron meteorites. Meteorit. Planet. Sci. 55 (12), 2758–2771.
Cook, D.L., Meyer, B.S., Schönbächler, M., 2021. Iron and nickel isotopes in IID and IVB iron meteorites: evidence for admixture of an SN II component and implications for the initial abundance of ^{60}Fe. Astrophys. J. 917 (2), 59.
Corrigan, C.M., Nagashima, K., Hilton, C., McCoy, T.J., Ash, R.D., Tornabene, H.A., Walker, R.J., McDonough, W.F., Rumble, D., 2022. Nickel-rich, volatile depleted iron meteorites: relationships and formation processes. Geochim. Cosmochim. Acta 333, 1–21.

Dauphas, N., Schauble, E.A., 2016. Mass fractionation laws, mass-independent effects, and isotopic anomalies. Annu. Rev. Earth Planet. Sci. 44, 709–783.
Dauphas, N., Marty, B., Reisberg, L., 2002. Molybdenum nucleosynthetic dichotomy revealed in primitive meteorites. Astrophys. J. 569 (2), L139.
Fischer-Gödde, M., Burkhardt, C., Kruijer, T.S., Kleine, T., 2015. Ru isotope heterogeneity in the solar protoplanetary disk. Geochim. Cosmochim. Acta 168, 151–171.
Goldberg, E., Uchiyama, A., Brown, H., 1951. The distribution of nickel, cobalt, gallium, palladium and gold in iron meteorites. Geochim. Cosmochim. Acta 2 (1), 1–25.
Goldstein, J.I., Scott, E.R.D., Chabot, N.L., 2009. Iron meteorites: crystallization, thermal history, parent bodies, and origin. Geochemistry 69 (4), 293–325.
Goodrich, C.A., Berkley, J.L., 1986. Primary magmatic carbon in ureilites: evidence from cohenite-bearing metallic spherules. Geochim. Cosmochim. Acta 50 (5), 681–691.
Gramlich, J.W., Machlan, L.A., Barnes, I.L., Paulsen, P.J., 1989. Absolute isotopic abundance ratios and atomic weight of a reference sample of nickel. J. Res. Nat. Inst. Stand. Technol. 94 (6), 347.
Greenwood, R.C., Burbine, T.H., Miller, M.F., Franchi, I.A., 2017. Melting and differentiation of early-formed asteroids: the perspective from high precision oxygen isotope studies. Chemie der Erde – Geochem. 77, 1–43.
Grewal, D.S., Asimow, P.D., 2023. Origin of the superchondritic carbon/nitrogen ratio of the bulk silicate Earth–an outlook from iron meteorites. Geochim. Cosmochim. Acta 344, 146–159.
Hilton, C.D., Ash, R.D., Walker, R.J., 2022. Chemical characteristics of iron meteorite parent bodies. Geochim. Cosmochim. Acta 318, 112–125.
Hopp, T., Dauphas, N., Spitzer, F., Burkhardt, C., Kleine, T., 2022a. Earth's accretion inferred from iron isotopic anomalies of supernova nuclear statistical equilibrium origin. Earth Planet. Sci. Lett. 577, 117245.
Hopp, T., Dauphas, N., Abe, Y., Aléon, J., O'D. Alexander, C.M., Amari, S., Amelin, Y., Bajo, K.I., Bizzarro, M., Bouvier, A., Carlson, R.W., 2022b. Ryugu's nucleosynthetic heritage from the outskirts of the Solar System. Sci. Adv. 8 (46), eadd8141.
Jochum, K.P., Hintenberger, H., Buchwald, V.F., 1975. Distribution of minor and trace elements in the elongated troilite inclusions of the Cape York iron Agpalilik. Meteoritics 10, 419.
Jones, J.H., Drake, M.J., 1983. Experimental investigations of trace element fractionation in iron meteorites, II: the influence of sulfur. Geochim. Cosmochim. Acta 47 (7), 1199–1209.
Kleine, T., Budde, G., Burkhardt, C., Kruijer, T.S., Worsham, E.A., Morbidelli, A., Nimmo, F., 2020. The non-carbonaceous–carbonaceous meteorite dichotomy. Space Sci. Rev. 216, 1–27.
Kruijer, T.S., Sprung, P., Kleine, T., Leya, I., Burkhardt, C., Wieler, R., 2012. Hf–W chronometry of core formation in planetesimals inferred from weakly irradiated iron meteorites. Geochim. Cosmochim. Acta 99, 287–304.
Kruijer, T.S., Fischer-Gödde, M., Kleine, T., Sprung, P., Leya, I., Wieler, R., 2013. Neutron capture on Pt isotopes in iron meteorites and the Hf–W chronology of core formation in planetesimals. Earth Planet. Sci. Lett. 361, 162–172.
Kruijer, T.S., Touboul, M., Fischer-Gödde, M., Bermingham, K.R., Walker, R.J., Kleine, T., 2014. Protracted core formation and rapid accretion of protoplanets. Science 344 (6188), 1150–1154.
Kruijer, T.S., Burkhardt, C., Budde, G., Kleine, T., 2017. Age of Jupiter inferred from the distinct genetics and formation times of meteorites. Proc. Natl. Acad. Sci. 114 (26), 6712–6716.
Kruijer, T.S., Kleine, T., Borg, L.E., 2020. The great isotopic dichotomy of the early Solar System. Nat. Astron 4 (1), 32–40.
Liu, J., Qin, L., Xia, J., Carlson, R.W., Leya, I., Dauphas, N., He, Y., 2019. Cosmogenic effects on chromium isotopes in meteorites. Geochim. Cosmochim. Acta 251, 73–86.
Lovering, J.F., Nichiporuk, W., Chodos, A., Brown, H., 1957. The distribution of gallium, germanium, cobalt, chromium, and copper in iron and stony-iron meteorites in relation to nickel content and structure. Geochim. Cosmochim. Acta 11 (4), 263–278.
Makhatadze, G.V., Schiller, M., Bizzarro, M., 2023. High precision nickel isotope measurements of early Solar System materials and the origin of nucleosynthetic disk variability. Geochim. Cosmochim. Acta 343, 17–32.
Mathew, K.J., Marti, K., 2009. Galactic cosmic ray-produced ^{129}Xe and ^{131}Xe excesses in troilites of the Cape York iron meteorite. Meteorit. Planet. Sci. 44 (1), 107–114.
McDermott, K.H., Greenwood, R.C., Scott, E.R., Franchi, I.A., Anand, M., 2016. Oxygen isotope and petrological study of silicate inclusions in IIE iron meteorites and their relationship with H chondrites. Geochim. Cosmochim. Acta 173, 97–113.
Mougel, B., Moynier, F., Göpel, C., 2018. Chromium isotopic homogeneity between the Moon, the Earth, and enstatite chondrites. Earth Planet. Sci. Lett. 481, 1–8.
Nanne, J.A., Nimmo, F., Cuzzi, J.N., Kleine, T., 2019. Origin of the non-carbonaceous–carbonaceous meteorite dichotomy. Earth Planet. Sci. Lett. 511, 44–54.
Qin, L., Alexander, C.M.D., Carlson, R.W., Horan, M.F., Yokoyama, T., 2010. Contributors to chromium isotope variation of meteorites. Geochim. Cosmochim. Acta 74 (3), 1122–1145.
Regelous, M., Elliott, T., Coath, C.D., 2008. Nickel isotope heterogeneity in the early Solar System. Earth Planet. Sci. Lett. 272 (1–2), 330–338.
Render, J., Brennecka, G.A., Wang, S.J., Wasylenki, L.E., Kleine, T., 2018. A distinct nucleosynthetic heritage for early solar system solids recorded by Ni isotope signatures. Astrophys. J. 862 (1), 26.
Sanborn, M.E., Wimpenny, J., Williams, C.D., Yamakawa, A., Amelin, Y., Irving, A.J., Yin, Q.Z., 2019. Carbonaceous achondrites Northwest Africa 6704/6693: milestones for early Solar System chronology and genealogy. Geochim. Cosmochim. Acta 245, 577–596.
Schiller, M., Bizzarro, M., Siebert, J., 2020. Iron isotope evidence for very rapid accretion and differentiation of the proto-Earth. Sci. Adv. 6 (7), eaay7604.
Schoenberg, R., von Blanckenburg, F., 2005. An Assessment of the Accuracy of Stable Fe Isotope Ratio Measurements on Samples with Organic and Inorganic Matrices by High-Resolution Multicollector ICP-MS. Int. J. Mass Spectrom. 242, 257–272.
Scott, E.R., Wasson, J.T., Buchwald, V.F., 1973. The chemical classification of iron meteorites—VII. A reinvestigation of irons with Ge concentrations between 25 and 80 ppm. Geochim. Cosmochim. Acta 37 (8), 1957–1983.
Scott, E.R., Wasson, J.T., 1975. Classification and properties of iron meteorites. Rev. Geophys. 13 (4), 527–546.
Shields, W.R., Murphy, T.J., Catanzaro, E.J., Garner, E.L., 1966. Absolute isotopic abundance ratios and the atomic weight of a reference sample of chromium. J. Res. Natl. Bureau Stand. Sect. A: Phys. Chem. 70A, 193–197.
Shima, M., Honda, M., 1966. Distribution of spallation produced chromium between alloys in iron meteorites. Earth Planet. Sci. Lett. 1 (2), 65–74.
Smith, T., Cook, D.L., Merchel, S., Pavetich, S., Rugel, G., Scharf, A., Leya, I., 2019. The constancy of galactic cosmic rays as recorded by cosmogenic nuclides in iron meteorites. Meteorit. Planet. Sci. 54 (12), 2951–2976.
Spitzer, F., Burkhardt, C., Budde, G., Kruijer, T.S., Morbidelli, A., Kleine, T., 2020. Isotopic evolution of the inner solar system inferred from molybdenum isotopes in meteorites. Astrophys. J. Lett. 898 (1), L2.
Spitzer, F., Burkhardt, C., Pape, J., Kleine, T., 2022. Collisional mixing between inner and outer solar system planetesimals inferred from the Nedagolla iron meteorite. Meteorit. Planet. Sci. 57 (2), 261–276.
Steele, R.C., Elliott, T., Coath, C.D., Regelous, M., 2011. Confirmation of mass-independent Ni isotopic variability in iron meteorites. Geochim. Cosmochim. Acta 75 (24), 7906–7925.
Tang, H., Dauphas, N., 2012. Abundance, distribution, and origin of ^{60}Fe in the solar protoplanetary disk. Earth Planet. Sci. Lett. 359, 248–263.
Trinquier, A., Birck, J.L., Allegre, C.J., 2007. Widespread ^{54}Cr heterogeneity in the inner solar system. Astrophys. J. 655 (2), 1179.
Trinquier, A., Birck, J.L., Allègre, C.J., 2008a. High-precision analysis of chromium isotopes in terrestrial and meteorite samples by thermal ionization mass spectrometry. J. Anal. At. Spectrom 23 (12), 1565–1574.
Trinquier, A., Birck, J.L., Allègre, C.J., Göpel, C., Ulfbeck, D., 2008b. ^{53}Mn–^{53}Cr systematics of the early Solar System revisited. Geochim. Cosmochim. Acta 72 (20), 5146–5163.
Walker, R.J., 2012. Evidence for homogeneous distribution of osmium in the protosolar nebular. Earth Planet. Sci. Lett. 315–352, 36–44.
Wang, P.L., Rumble III, D., McCoy, T.J., 2004. Oxygen isotopic compositions of IVA iron meteorites: implications for the thermal evolution derived from in situ ultraviolet laser microprobe analyses. Geochim. Cosmochim. Acta 68 (5), 1159–1171.
Warren, P.H., 2011. Stable-isotopic anomalies and the accretionary assemblage of the Earth and Mars: a subordinate role for carbonaceous chondrites. Earth Planet. Sci. Lett. 311 (1–2), 93–100.
Wasson, J.T., 1967. The chemical classification of iron meteorites: I. A study of iron meteorites with low concentrations of gallium and germanium. Geochim. Cosmochim. Acta 31 (2), 161–180.
Wasson, J.T., 1974. Meteorites-Classification and Properties. Springer, New York, p. 316.
Wasson, J.T., Choe, W.H., 2009. The IIG iron meteorites: probable formation in the IIAB core. Geochim. Cosmochim. Acta 73 (16), 4879–4890.
Wasson, J.T., Kimbeblin, J., 1967. The chemical classification of iron meteorites—II. Irons and pallasites with germanium concentrations between 8 and 100 ppm. Geochim. Cosmochim. Acta 31 (10), 2065–2093.
Wasson, J.T., Huber, H., Malvin, D.J., 2007. Formation of IIAB iron meteorites. Geochim. Cosmochim. Acta 71 (3), 760–781.
Wittig, N., Humayun, M., Brandon, A.D., Huang, S., Leya, I., 2013. Coupled W-Os–Pt isotope systematics in IVB iron meteorites: in situ neutron dosimetry for W isotope chronology. Earth Planet. Sci. Lett. 361, 152–161.
Worsham, E.A., Bermingham, K.R., Walker, R.J., 2017. Characterizing cosmochemical materials with genetic affinities to the Earth: genetic and chronological diversity within the IAB iron meteorite complex. Earth Planet. Sci. Lett. 467, 157–166.
Worsham, E.A., Burkhardt, C., Budde, G., Fischer-Gödde, M., Kruijer, T.S., Kleine, T., 2019. Distinct evolution of the carbonaceous and non-carbonaceous reservoirs: insights from Ru, Mo, and W isotopes. Earth Planet. Sci. Lett. 521, 103–112.
Yamakawa, A., Yamashita, K., Makishima, A., Nakamura, E., 2009. Chemical separation and mass spectrometry of Cr, Fe, Ni, Zn, and Cu in terrestrial and extraterrestrial materials using thermal ionization mass spectrometry. Anal. Chem. 81 (23), 9787–9794.
Yamakawa, A., Yamashita, K., Makishima, A., Nakamura, E., 2010. Chromium isotope systematics of achondrites: chronology and isotopic heterogeneity of the inner solar system bodies. Astrophys. J. 720 (1), 150.
Zhang, B., Chabot, N.L., Rubin, A.E., 2024. Compositions of iron-meteorite parent bodies constrain the structure of the protoplanetary disk. Proc. Natl. Acad. Sci. 121 (23), e2306995121.
Zhu, K., Moynier, F., Schiller, M., Wielandt, D., Larsen, K.K., van Kooten, E.M., Barrat, J. A., Bizzarro, M., 2020. Chromium isotopic constraints on the origin of the ureilite parent body. Astrophys. J. 888 (2), 126.